Offshore wind power simulation by using WRF in the central coast of Chile

Article *in* Renewable Energy · August 2016

DOI: 10.1016/j.renene.2016.03.005

2 authors, including:

Cristian Mattar

University of Chile

69 PUBLICATIONS **340** CITATIONS

SEE PROFILE

Renewable Energy 94 (2016) 22–31

Contents lists available at ScienceDirect

Renewable Energy

journal homepage: www.elsevier.com/locate/renene

Offshore wind power simulation by using WRF in the central coast of Chile

Cristian Mattar*, Dager Borvarán

Laboratory for Analysis of the Biosphere (LAB), Department of Environmental Sciences and Renewable Natural Resources, University of Chile, Av. Santa Rosa 11315, Santiago, Chile

ARTICLE INFO

Article history:
Received 1 October 2015
Received in revised form
30 January 2016
Accepted 2 March 2016

Keywords:
Wind simulation
Offshore
Wind power
WRF
Chile

ABSTRACT

This paper presents the first estimate of offshore wind power potential for the central coast of Chile. For this purpose, wind speed data from in-situ stations and ERA-Interim reanalysis were used to simulate wind fields at regional level by means of the Weather Research and Forecasting (WRF) model. Wind field simulations were performed at different heights (20, 30, 40 and 140 m.a.s.l.) and a spatial resolution of 3×3 km for the period from February 1, 2006 to January 31, 2007, which comprised the entire series of in-situ data available. The results show an RMSE and r^2 of 2.2 m s^{-1} and 0.55 respectively for the three heights simulated as compared to in-situ data. Based on the simulated wind data, the wind power for the study area was estimated at ~1000 W m^{-2} at a height of 140 m.a.s.l. For a typical wind turbine of 8 MW generator, the estimated capacity factor exceeds 40%, with an average annual generation of ~30 GWh. Offshore wind power in Chile is an emerging renewable energy source that is as yet still underdeveloped, these estimates help to fill in some of the gaps in our knowledge about Chile's true renewable energy potential.

1. Introduction

New sources of power generation that reduce greenhouse gas emissions, such as renewable energy, have seen significant growth worldwide. As a part of this, wind power appears to be one of the most commonly used renewable power sources nowadays [1], with exponential growth in its installed capacity worldwide and a growth rate of 33 GW $year^{-1}$ for the period 2004–2014 [2]. This growth, mainly in installed capacity at global level, has been driven by not only onshore wind energy, but by offshore wind power as well.

The business of offshore wind energy has been also growing significantly since the early 2000 generating more power than onshore (i.e. capacity factor over 40%), with greater power from each generator and a decrease in the investment costs of wind power projects [3–6]. At the same time, trends point toward developing wind farms with greater power and area compared to those existing today, as well as installations in deeper waters on floating and semi-submersible structures [6–9].

The quantification of offshore wind power is a necessary first step in any power generation project. To do this, in-situ measurements are required, though not always available and often insufficient for the successful development of wind projects. For this reason, the lack of in-situ measurements of the ocean surface forces us to look to different usable sources of information about wind fields on the sea surface [10]. These sources of information can come from remote sensing (i.e. QuickSCAT, WindSat, Ers, ASCAT, ASAR) [11–13], from simulated data using prediction models (Numerical Weather Prediction), analysis/reanalysis (i.e. GFL, ERA-Interim) [14,15] or a combination, such as in-situ, satellite and modeling [16–18]. This combined use of different data sources and modeling has been widely employed in areas where there is an extensive network of in-situ data, resulting in the use of mesoscale forecasting models such as today's most commonly used Weather Research and Forecasting Model (WRF) [16,19–24]. Such methodologies (i.e. in-situ data, models and reanalysis) might aid developing countries prospecting for wind power and other future renewable sources to meet their energy needs, now and in the future.

One such country is Chile, which has over 4000 km of coastline and the second largest installed wind power capacity in South America (e.g. 833 MW) in 2014, as well as newly passed energy legislation (Law 20 698/2013) aiming for electricity consumption

* Corresponding author..
E-mail address: cmattar@uchile.cl (C. Mattar).

http://dx.doi.org/10.1016/j.renene.2016.03.005
0960-1481/

from renewable sources to reach 20% by 2020. This scenario has led to several studies quantifying Chile's onshore wind potential [25–27]. Offshore wind power, however, has not yet been widely analyzed. In fact the only work that has focused on estimating offshore wind potential was published by Mattar and Villar-Poblete [28] using data from QuikSCAT and ERA-Interim reanalysis. Due to the spatial resolution of the two data sets though, wind power potential was estimated at a low spatial resolution, thus creating an alternative for improving the estimation of this potential for Chile's coastline. Hence, the aim of this study was to estimate the offshore wind power potential with improved spatial resolution off the coast of south-central Chile using wind data simulated by the WRF model. The structure of this paper is detailed as follows. Section 2 defines the study area and in-situ wind measurements. Section 3 presents the modeling system, section 4 shows the method, section 5 provides the study results and sections 6 and 7 provide a discussion and final conclusion for this paper, respectively.

2. Study area and in-situ data

The study area is located in south-central Chile (Fig. 1), encompassing the coast of the southern section of the Maule Region, to a distance of 100 km from the coastline. The study area located on the earth's surface is made up of a flat inland area and mountainous coast. The winds in this area are influenced by the presence of the Southeast Pacific anti-cyclone, which mainly produces winds originating in the south [29]. Within the study area can be found the Faro Carranza Station (FCS) (S 35°32′32.3″ W 72°35′20.9″), which was installed by the National Energy Commission between January 29, 2006 and June 8, 2007 [30]. This station is located in a barren area (sandy) located at 30 m from the sea coast line. This coastal area has shown potential for high wind [25,26] though studies in this area have focused on the estimation of onshore wind power, so its offshore wind power is unknown and its power could far exceed estimates for onshore.

For this paper, FCS data were used for the assessment of wind simulations using the WRF. The FCS data consist of wind speed and direction measurements recorded each 10 min at heights of 20, 30 and 40 m and 20 m respectively, were used for the entire period that the station recorded data, which it did continuously for one year.

3. WRF modeling system

For this paper, version 3.6 of the WRF model was used [31]. A configuration of three nested domains at spatial resolutions of 27, 9 and 3 km (Fig. 2) was used and information was exchanged between each domain during the simulations using a two way nested run. The physical configuration used in the simulation was defined as the default configuration detailed as follows: WSM3 for microphysics, RRTM for longwave radiation, Dudhia on shortwave radiation, YSU for boundary layer, Monin–Obukhov for surface layer and Noah- LSM for land use. Previous WRF simulation were carried out in Chile including some minor modification from the default configuration using in the microphysic parametrization without any previous sensitivity analysis since the lack of in-situ data [27,32]. The information used to configure the initial state of the atmosphere and boundary conditions were obtained in the WRF model through ERA-Interim reanalysis [33] for the simulation period 1 February 2006–31 January 2007, which matches the data measured by the FCS. Global ERA-Interim data are available for 1979 to the present, at a time resolution of 6 h and spatial

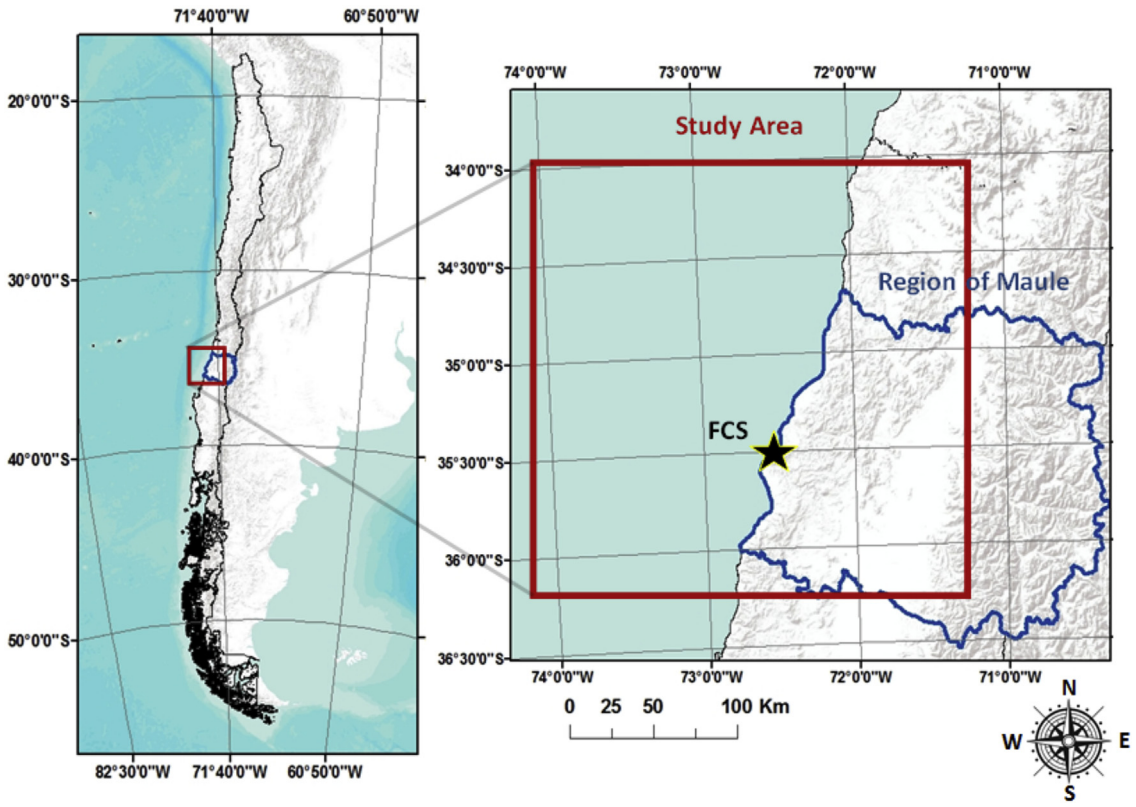

Fig. 1. Study area (red square) located in the Maule region (blue line), Chile. The FCS is indicated by a star. Grey colors indicate the relief of the zone. (For interpretation of the references to colour in this figure legend, the reader is referred to the web version of this article.)

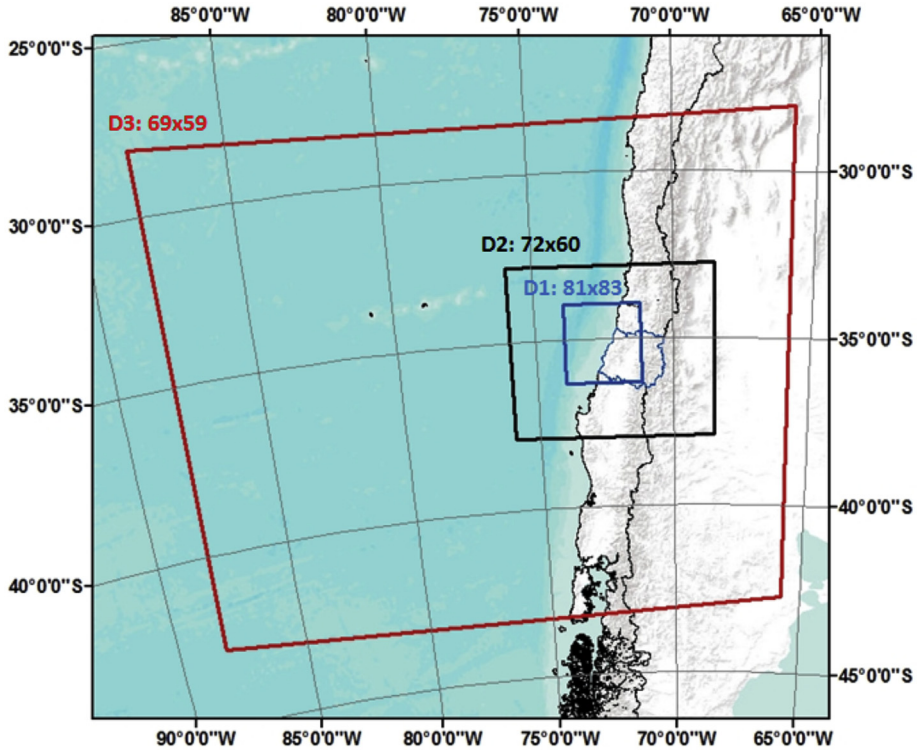

Fig. 2. Simulation domains used in this study. The color red corresponds to the outermost domain, black is the medium domain and blue corresponds to the innermost domain. (For interpretation of the references to colour in this figure legend, the reader is referred to the web version of this article.)

resolution of 0.75° × 0.75° (latitude–longitude). In terms of its vertical configuration, this study used 37 atmospheric levels ranging from 1000 to 1 hPa. For previous work, ERA-interim data have been used in studies on wind energy, providing robust and reliable results for this type of application in offshore wind energy [21,22,34,35]. The model's output data for the study area were generated at 3 km spatial resolution every 1 h for the period between 1 February 1 2006 and 31 January 2007 at 33 vertical levels, ensuring that the first 3 levels were less than 100 m above ground.

4. Methods

4.1. Estimating the profile of the wind speed module through WRF

Using the gridlines and the non-staggered horizontal components *U* and *V* of the wind speed simulated by the WRF at the first five vertical levels provided by the model (5, 24, 50, 110 and 222 m approx.), the wind speed magnitude was calculated for each of those levels (1).

$$\overline{v_z} = \sqrt{U_z^2 + V_z^2}, \quad z = \sim 5, \sim 24, \sim 50, \sim 110\, y \sim 222m \qquad (1)$$

This wind speed module at the first five levels was interpolated at the next vertical levels 20, 30, 40 and 140 m by means of a spline interpolation in order to compare the magnitudes of the speeds recorded at the FCS ($\overline{v}_{obs_{Z_{FCS}}}$) and the simulations performed with WRF for the FCS location ($\overline{v}_{WRF_{Z_{FCS}}}$). This was done for the three vertical levels measured at the station ($Z_{FCS} = 20, 30y\ 40\ m$). It was assumed a normal distribution of the simulated and observed data and a statistical significance level equal to 95%. This comparison was performed using the coefficient of determination (r^2) (2), the bias (3) derived from the residuals between observed and simulated and the Root Mean Square Error (RMSE) (4) at annual, seasonal and monthly level, for Z_{FCS}. These equations are detailed as follows.

$$r^2_{Z_{FCS}} = \frac{S_{\overline{v}_{obs_{Z_{FCS}}}\overline{v}_{WRF_{Z_{FCS}}}}}{S_{\overline{v}_{obs_{Z_{FCS}}}} S_{\overline{v}_{WRF_{Z_{FCS}}}}}^2 \qquad (2)$$

$$BIAS_{Z_{FCS}} = \frac{1}{N}\sum_{i=1}^{N} \overline{v}_{obs_{Z_{FCS}}} - \overline{v}_{WRF_{Z_{FCS}}} \qquad (3)$$

$$RMSE_{Z_{FCS}} = \sqrt{\frac{1}{N}\sum_{i=1}^{N}\left(\overline{v}_{obs_{Z_{FCS}}} - \overline{v}_{WRF_{Z_{FCS}}}\right)^2} \qquad (4)$$

Where N is the number of pair of data between observed and estimated.

4.2. Estimation of wind power potential

The wind power was calculated using the probability distribution for wind speeds estimated at a height of 140 m ($\overline{v}_{z140}$), which was calculated using the Weibull distribution function. The Weibull function (5) is defined by the shape parameters (k) and the scale parameter (c), which were calculated using the method of least square [36]. This was performed for each pixel of the study area.

$$f(\overline{v}_{z140}) = \frac{k}{c}\left(\frac{\overline{v}_{z140}}{c}\right)^{k-1} \exp\left[-\left(\frac{\overline{v}_{z140}}{c}\right)^{k}\right] \qquad (5)$$

Once the distribution function of the wind speed was known, the wind power (6) was calculated with the following equation:

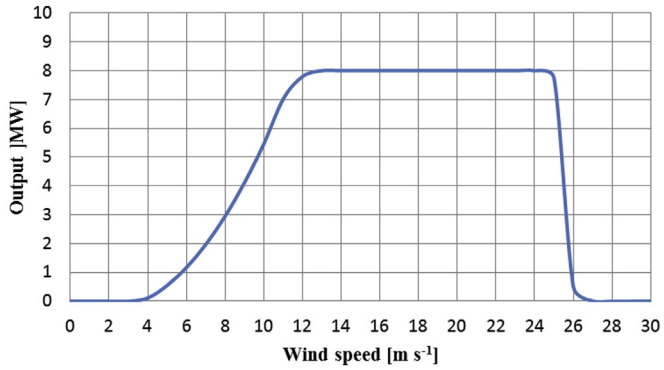

Fig. 3. Power curve for the turbine V164 (adapted from Vestas[1]).

The annual average power produced by the wind turbine (7) was estimated. Estimated wind speeds at 140 m elevation were used, this being the height of the wind turbine's operation. The annual average power produced by the wind turbine is based on the likelihood of occurrence ($f(\bar{v}_{z140})$) and wind turbine power $p(\bar{v}_{z140})$ at each of the simulated speeds:

$$P^* = \int_0^\infty p(\bar{v}_{z140}) f(\bar{v}_{z140}) d\bar{v}_{z140} \tag{7}$$

Then, from the annual average power, the energy generation for the period simulated was estimated ($T = 8760$ h) (8).

$$E = P^* * T \tag{8}$$

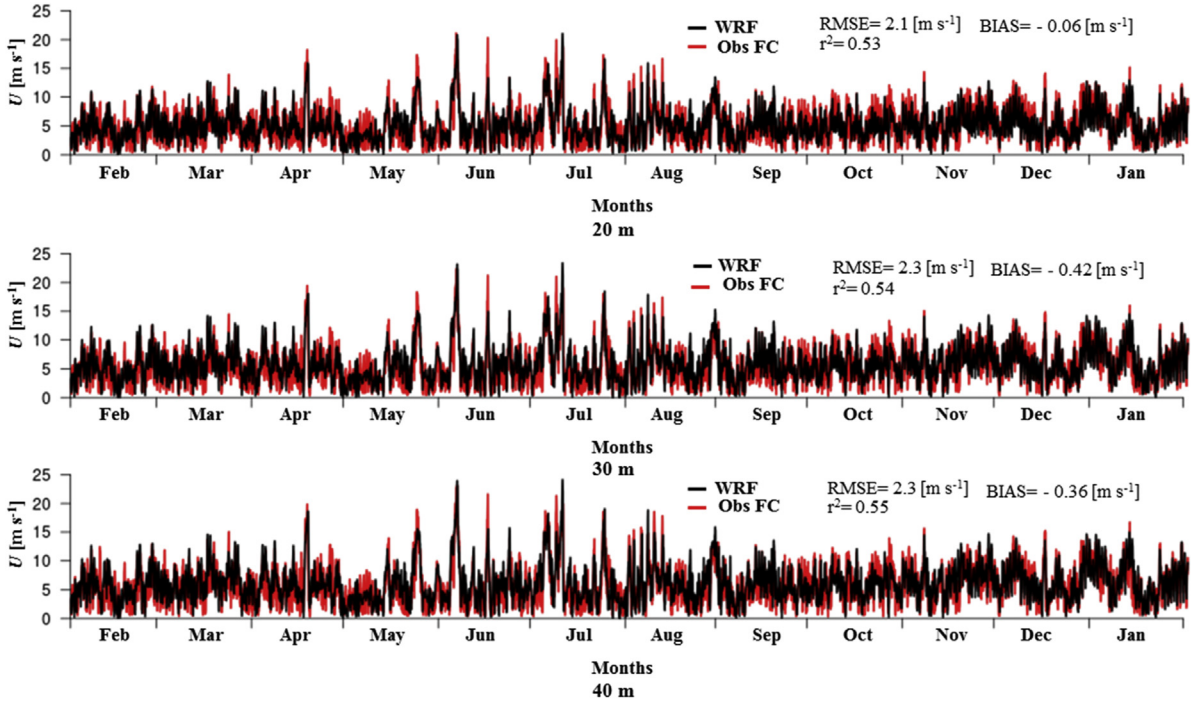

Fig. 4. Time series for speeds simulated by WRF and those recorded at the Faro Carranza station at 20, 30 and 40 m.

$$\frac{\overline{P}}{A} = \frac{1}{2}\rho \int_0^\infty v_{z140}^3 f(\bar{v}_{z140}) d\bar{v}_{z140} \tag{6}$$

Where ρ is the air density, which for this study was considered to be constant, equal to 1.225 kg m^{-3}.

4.3. Capacity factor and energy production

In order to estimate offshore wind energy potential, the energy that could be generated in this area by a V164-8.0 (V164) wind turbine was estimated. This wind turbine has a rated power (P_n) of 8 MW, making it one of the more powerful wind turbines available on the market today. The power curve of the wind turbine is shown in Fig. 3, where it can seen that its rates of cut in wind speed, rated wind speed and cut out wind speed are 4, 12 and 25 m s^{-1} respectively.

The Hours at Full Capacity (HFC) was also estimated since this metric is often the most important to wind energy operators, since it translates the relation between the wind farm installation and exploration cost and net production.

$$HFC = \frac{E}{P_n} \tag{9}$$

The efficiency of the wind turbine (11) was estimated by using the energy generation, wind power, area covered by the rotor turbine (10) and T.

$$A_{V164-8.0} = \pi * r_{V164-8.0}^2,\ r_{V164-8.0} = 80\ m \tag{10}$$

$$Efficiency = \frac{E}{\frac{\overline{P}}{A} * A_{V164-8.0} * T} \tag{11}$$

Finally, the capacity factor (CF) was calculated from the relationship between the energy generated and the maximum amount of energy that could be produced over an average year ($P_n * T$):

[1] http://nozebra.ipapercms.dk/Vestas/Communication/Productbrochure/OffshoreProductBrochure/OffshoreProductBrochure.

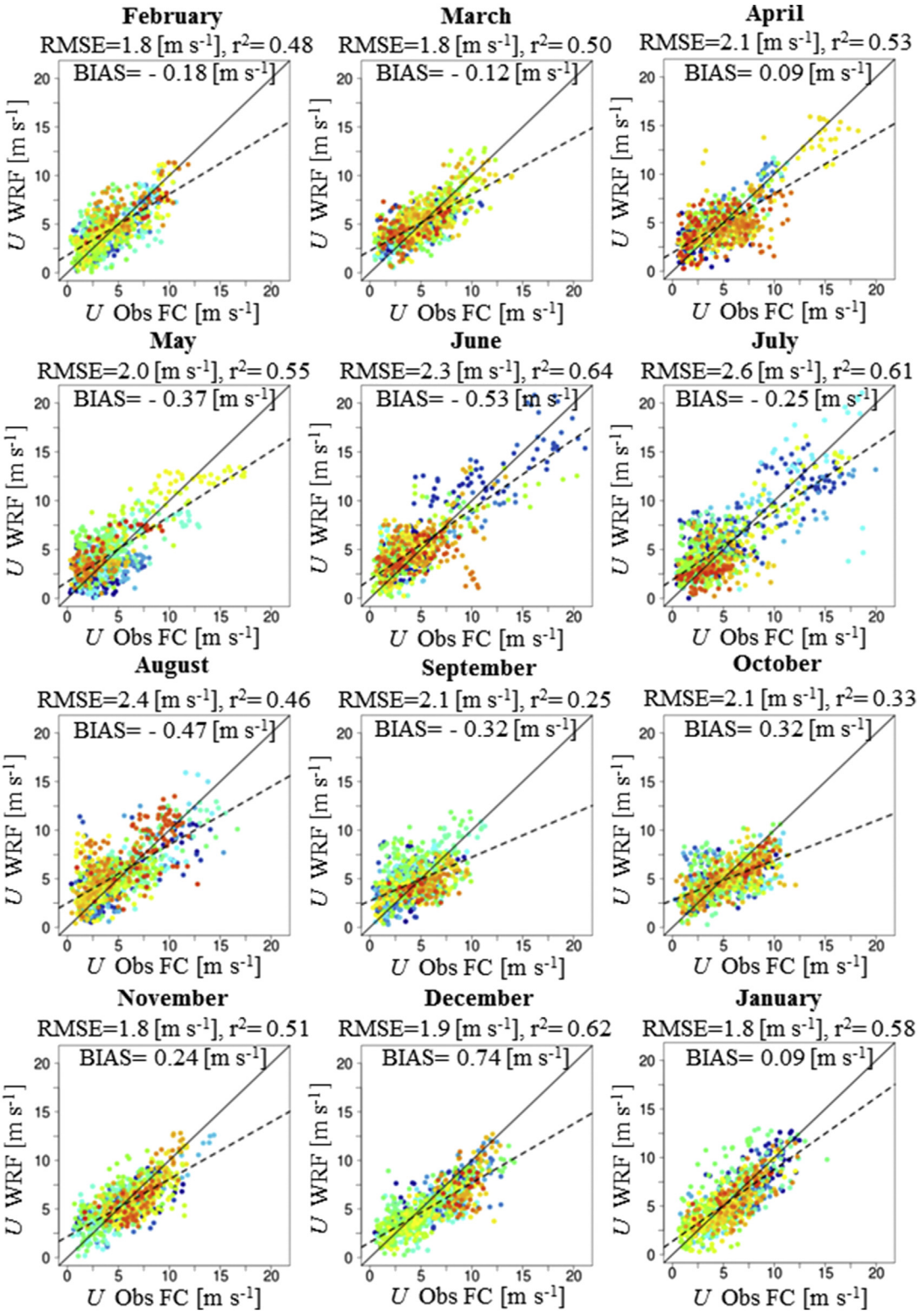

Fig. 5. Density graphs of the simulated speed vs recorded speed at the FCS for the 12 months simulated at a height of 20 m. Blue and red represent values with lower and higher frequency, respectively. (For interpretation of the references to colour in this figure legend, the reader is referred to the web version of this article.)

$$CF = \frac{E}{P_n * T} \tag{12}$$

All variables listed above were assumed for each pixel by considering there to be one wind turbine per spatial unit (3 × 3 km) for the entire study area.

5. Results

5.1. Assessment of the wind speed and direction simulated at FCS

The time series for wind speeds simulated by WRF for the FCS location and in-situ records for the entire simulation period at 20,

Table 1
RMSE and r^2 values by season at heights of 20, 30 and 40 m.

Period		RMSE [m s^{-1}]			r^2		
		20 m	30 m	40 m	20 m	30 m	40 m
Seasonal	Summer	1.8	1.9	2.0	0.65	0.57	0.57
	Autumn	2.0	2.2	2.2	0.54	0.55	0.56
	Winter	2.5	2.7	2.8	0.58	0.59	0.61
	Spring	2.0	2.2	2.2	0.38	0.39	0.40

30 and 40 m can be found in Fig. 4. The speeds simulated by WRF follow the speed patterns recorded in the FCS, with an average coefficient of determination of 0.54, which does not vary greatly with altitude. The same can be said for RMSE, which is equal to 2.1 m s^{-1}, 2.3 m s^{-1} and 2.3 m s^{-1} at 20, 30 and 40 m, respectively. For the period from April to August, the maximum recorded wind speed values (between 15 and 25 m s^{-1}) coincide with those simulated by WRF. However, certain values may tend to be underestimated due to the existence of local phenomena, about which WRF might need additional information in order for it to be represented. From a monthly perspective, Fig. 5 shows the density of the speeds simulated by WRF for the FCS location and the speed recorded at the station at 20 m. In average, the wind speed simulated at 20 m by using WRF present an underestimation in comparison to FCS data. The RMSE grouped by month varies between 1.8 m s^{-1} recorded in the months of February, March, November and January, while the month with the highest RMSE, July, is close to 2.6 m s^{-1}. Regarding the coefficient of determination, this range from 0.25 for the month of September to 0.64 for the month of June, while in July and December the coefficient of determination also reaches values of around 0.6. The situation for July (maximum RMSE) may be related to certain outliers measured in-situ that the modeling cannot deliver, thus recording differences in the simulated wind speed of around 15 m s^{-1}. In general, every month has large amplitude for the simulated and measured wind values, ranging between 0 and 25 m s^{-1}. However, for the month of September, it can be observed that most of the values fall below 10 m s^{-1}, which might influence the linear correlation between the WRF simulated values and the FCS measured data. At heights of 30 and 40 m, results were similar to those found at 20 m, except that higher magnitudes of RMSE and r^2 were recorded, though not statistically significant ($p < 0.05$).

Table 1 shows the RMSE and r^2 values by season at 20, 30 and 40 m obtained for FCS location. For the seasonal series, which considers summer (December, January and February), autumn (March, April and May), winter (June, July and August) and spring (September, October and November), it was observed that in most cases, the value of both statistics (RMSE and r^2) increases with height, though not significantly ($p > 0.05$). For the seasonal series, summer was the season that recorded the lowest RMSE, which varies between 1.8 and 2 m s^{-1} and increases according to height, with r^2 of 0.65 and 0.57 at 20 and 40 m respectively. Winter on the other hand had the highest RMSE, reaching values of 2.5 and 2.8 m s^{-1} at 20 and 40 m respectively, and r^2 of 0.58 and 0.61 at 20 and 40 m respectively. The fall and spring seasons showed similar RMSE values 2.0 and 2.2 m s^{-1} at 20 and 40 m. However, the r^2 values during spring were the lowest, coming in at 0.38 at 20 m and 0.40 at 40 m, while for autumn these values ranged from 0.54 to 0.56 at 20 and 40 m respectively. The RMSE values are similar at different heights for every season except summer at 20 m.

The simulated and measured wind directions are showed Fig. 6 where the South and SW direction are similar in frequency and magnitude. Moreover, similar patterns are also shown in NE direction founded similar frequency and wind speed magnitude. Despite the good results, in average, of the simulated and measured wind direction, certain discrepancies appears in the SE direction where WRF simulates wind speed where the frequency is slightly higher than 7%, although FCS did not present any frequency or even speed magnitude in such direction.

5.2. Wind fields simulations

The mean monthly wind field simulation for the study area at 20 m can be found in Fig. 7. This shows that the wind speeds are greater over the sea as compared to those over land, with major differences for the months of March, April, November and January. In general, the months with higher simulated wind speeds were March, April, November and January, which reached values of around 10 m s^{-1} for the offshore zone, while in May, June and July,

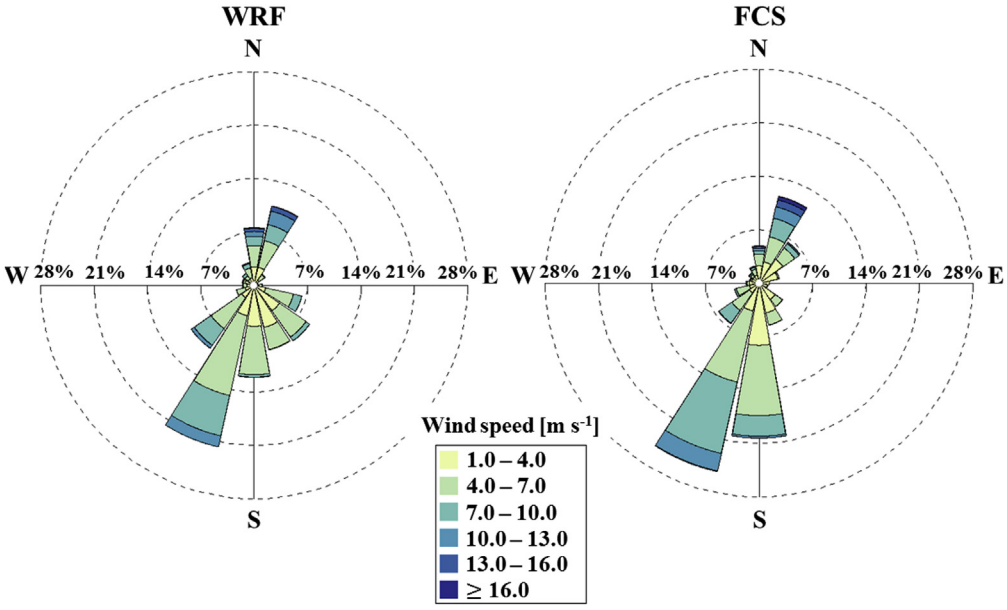

Fig. 6. Simulated and observed wind direction at Faro Carranza Station.

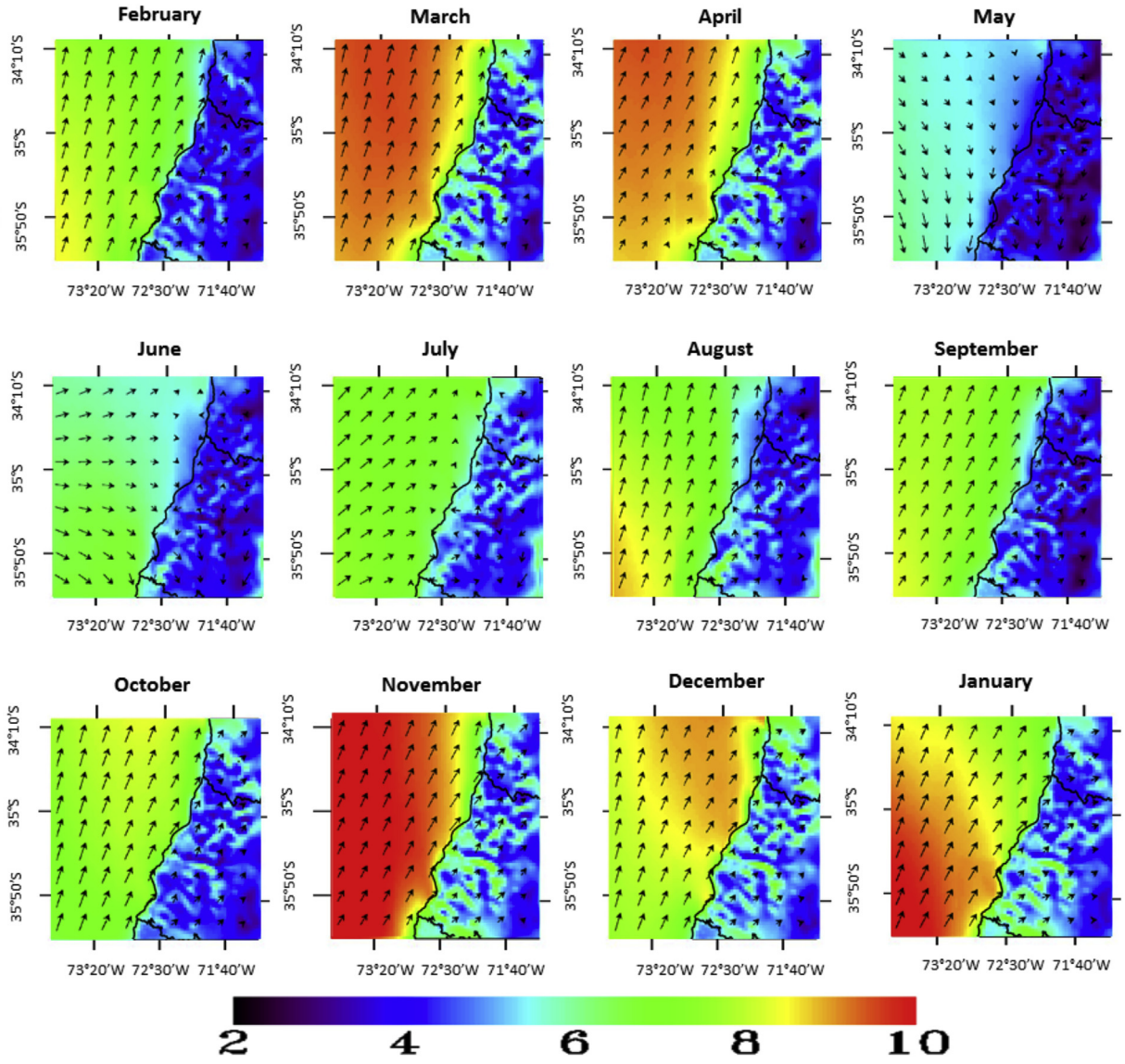

Fig. 7. Mean monthly wind fields [m s^{-1}] for the simulated period within the study area at 20 m.

the lowest wind speeds were simulated, reaching mean values of 5 m s^{-1}. Within the onshore area, the wind speed of least magnitude can be found in the south–east (2 m s^{-1} in January) which matches with the flat inland area, while the northeast shows the highest values (6 m s^{-1} in March, April, November and December) where the coastal mountain range is located. The winds within the offshore area increase the further away from the coast they are, though this gradient is accentuated north of 35°S, where values on the order of 3 m s^{-1} are shown near the coast during the month of May and 10 m s^{-1} for the months of March, April and November roughly 100 km from the coast. South of 35°S, wind speed values are higher, ranging from 6 to 10 m s^{-1} for May and March respectively. In terms of wind direction, most of months present the same pattern (south–north), although different results were obtained during May which presents an opposite direction (north–south) and the months of June and July, where the wind direction came from the west. There is important to denote that these months coincide with the minimum ranges of simulated wind speed off and onshore. The onshore wind field direction presented in this work differs from the published in Morales et al. [26] for the months of

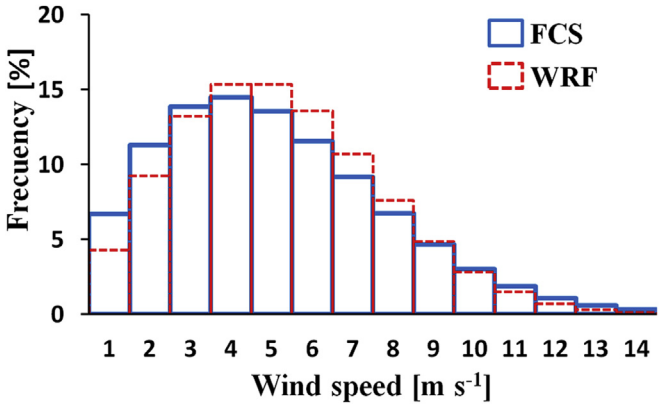

Fig. 8. Frequency distribution (in percentage) of the wind speed (m s^{-1}) simulated by WRF and measured FCS.

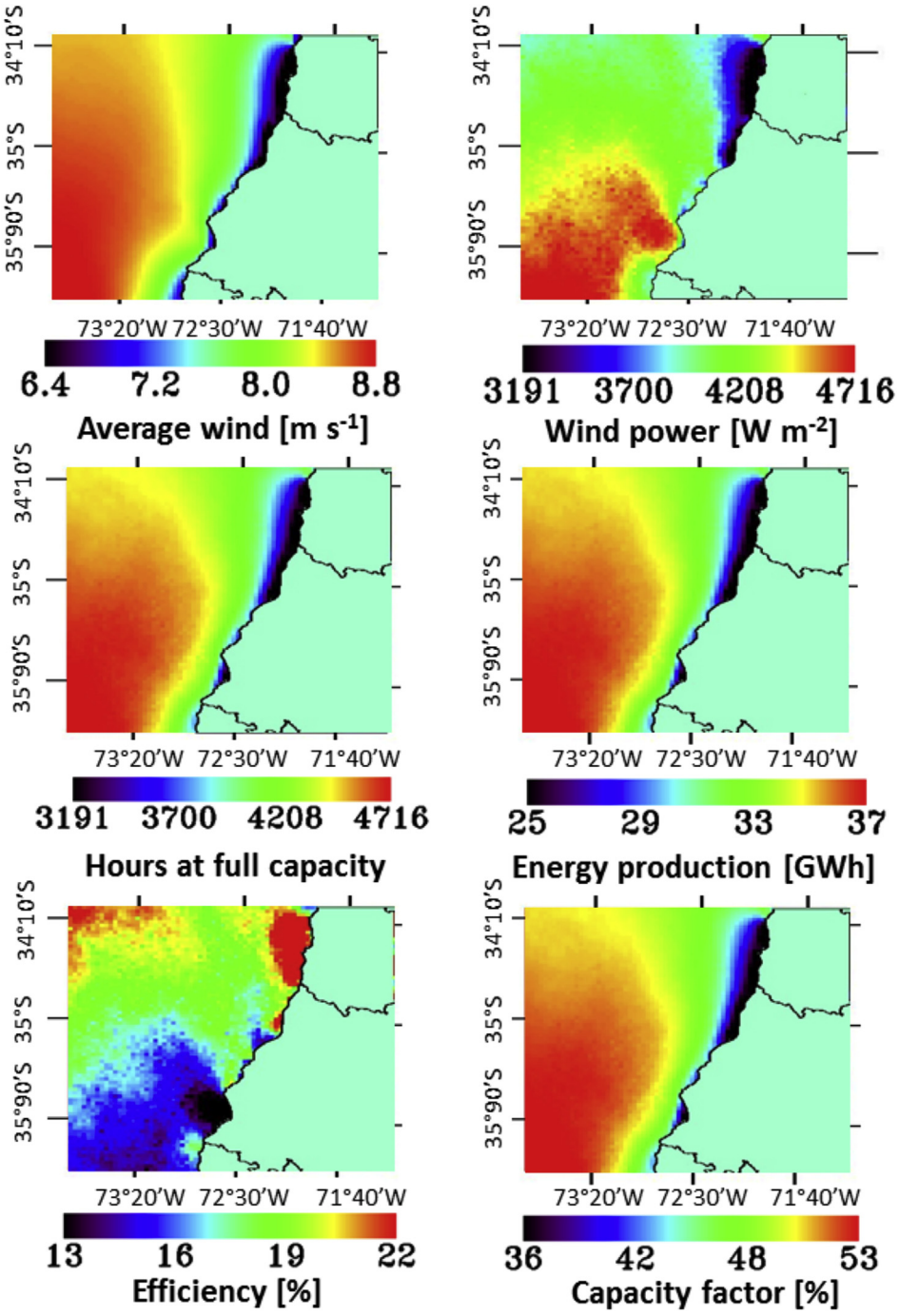

Fig. 9. Average annual speed [m s^{-1}] and wind power [W m^{-2}] estimated at height of 140 m, along with HFC, annual generated energy [GWh], efficiency [%] and capacity factor [%] for the V164.

winter because of that work used a different data set and methodology such as wind speed components from NCEP NCAR reanalysis at 2.5 × 2.5°, mathematic interpolation based method derived from kriging which could impact the spatial variations of wind speed in addition of the higher spatial resolution in the simulation of CALMET model (1 × 1 km).

5.3. Offshore wind power potential

The comparison between wind speed distribution frequency is presented in Fig. 8. Both distribution show similar patterns presenting the highest wind speed occurrence at 4 m s^{-1}. However, the wind speed frequency simulated by WRF tend to be higher than FCS between 5 and 8 m s^{-1} in contrast to the range between 1 and 3 where the WRF simulated a distribution frequency lower than FCS. For the lowest frequencies (wind speed higher than 9 m s^{-1}) there is no statistical difference between WRF and FCS ($p < 0.05$).

Fig. 9 shows the average annual wind speed and wind power at 140 m within the study area, along with estimations in energy production, HFC, efficiency and capacity factor for the V164. It can be seen that for much of the offshore area, there are average annual speeds of around 7 m s^{-1}. The simulated wind power for the study

Table 2
RMSE and r^2 obtained in studies using WRF to simulate wind speeds in wind energy applications.

RMSE [m s^{-1}]	r^2	WRF four dimensional data assimilation	Period of simulation	Author
2.07–2.62	–	No	5 years	Dvorak et al. [16]
3.09–3.72	–	Yes	1 month	Carvalho et al. [39]
1.7–3.7	0.79–0.90	Yes	1 year	Carvalho et al. [34,21]
1.85–2.53	0.70–0.88	Yes	1 year	Carvalho et al. [20,22]
1.56–3.42	–	No	4 days	Muñoz-Esparza et al. [40]
_	0.61–0.77	No	2 days and 1 month	Giannakopoulou and Nhili [35]
_	0.76–0.83	No	4 years	Peña et al. [41]

area ranges between 745 and 1240 W m^{-2}, with values of 900 W m^{-2} to the north of 35 °S, and values of around 1200 W m^{-2} to the south of 35 °S. The simulated capacity factor is practically about 40% across the entire offshore area, reaching values of around 50% at 50 km from the coast for the area located south of 35°S. The HFC simulated for V164 range between 3191 and 4716 located at northern and southern 35°S, respectively. As for estimated power generation, this comes to about 29 GWh, and close to 37 GWh for the offshore area adjacent to the FCS. Lastly, the efficiency simulated for V164, the lower values were estimated in the coast near the FCS and the maximum values of efficiency are close to 35 °S.

6. Discussion

The RMSE and r2 obtained for the comparison between WRF and FCS did not show any direct relationship which can be attributed to seasonal or spatial patterns. Nevertheless, it seems that the proximity of FCS to the coast line (~30 m) can present some local influences in the wind speed that WRF could not simulate at 3 × 3 km. However, the RMSE is mostly attributed to the standard deviation than the bias derived from the residuals between observed and simulated wind speed at FCS. For instance, the period between April–October the RMSE is higher than 2 m s^{-1}. The r^2 might changes with the linear dispersion of the maximum and minimum values of wind speed which is higher during June and July.

The wind simulation values obtained from the WRF were similar in both RMSE and r^2 when compared to similar studies (Table 2). In fact, it is possible to see that the speeds obtained in the simulations have relatively similar errors to those in studies of these characteristics, as far as RMSE. As for the r^2 values obtained in this study, these are of lower magnitude than those obtained in other studies. While it is true that the RMSE found in this study are within the range found in other studies, the r^2 values are lower than in other studies perhaps as a result of different factors, such as local overestimation of certain wind speed values or the impact of in-situ data in the WRF simulation. For example, in some studies in which WRF overestimated wind speeds [37,38], the configuration that was used might have been what brought about this result. To analyze such possible effects on the simulated wind fields in the study area, various analyses on wind data sensitivity that takes into account different physical settings, such as those by Refs. [20,35,39] might provide important information for developing further studies seeking to estimate wind potential through WRF modeling.

The capacity factor obtained in the study area for the V164 wind turbine is around 40% inside the entire offshore area and reaches values of around 50% at a distance over 50 km from the coast. These capacity factors are similar to those found at larger wind farm facilities in operation today (i.e Anholt 1, Avedøre Holme, Horns Rev I, Horns Rev II, Nysted (Rødsand) II, Rønland I, Samsø),[2] which have average annual values for energy generation and installed capacity of around 599.8 GWh and 1,46.7 MW. This demonstrates the advantages that the study area holds for the implementation of offshore wind energy and gives a first approximation of the amount of energy that might be generated in this area.

As for the estimated amount of energy generated for the study area, this is about 30 GWh. Energy production in Chile is currently at 1210.6 GWh, so the energy generated by a V164 wind turbine would represent 2.4% of the output of wind farms in Chile. However, this is a preliminary estimate and an estimate of future costs arising from the generation and delivery of consumable electricity is needed in order to assess the actual economic feasibility of generating offshore wind power in Chile in the future.

Based on the results presented in this work, WRF underestimate the wind speed values at comparing to FCS. Additional information from in-situ measurements, sea buoys or wind speed fuel derived from remote sensing such as SAR or ASCAT improve the simulation. Moreover, a sensitivity analysis related to the physical based model of WRF is also necessary to improve the simulations and to contribute to better understanding in the offshore wind potential.

7. Conclusion

In this study, wind fields were simulated using the WRF model for the central coastal area of Chile, which recorded average RMSE and r^2 values of 2.2 m s^{-1} and 0.55 respectively when compared to in-situ data measured at 20, 30 and 40 m. Despite underestimating the wind speed magnitude, possibly as a result of micro-scale effects, the WRF model showed its great potential in this type of exploratory studies on offshore wind power for areas where there is no large network of in-situ measurements. For this area of study, wind power was estimated to be high, ranging between 745 and 1240 W m^{-2} over the sea. The energy generation produced by a 8 MW wind turbine and over a pixel of 3 × 3 km was 30 GWh for the year that was simulated, with capacity factors of around 40%. This demonstrates the high potential that Chile's south-central area has for implementing offshore wind energy. Finally, this work contributes further relevant information on how new sources of renewable energy can be best used in developing countries, thus enabling the promotion of the kinds of renewable energy technologies that have had the greatest impact on the past decade worldwide.

Acknowledgments

The authors would like to thank the ECMWF for providing the ERA-Interim data, and the UCAR for providing the free delivery of the WRF model. The authors also thank to Dr. Jorge Navarro at CIEMAT for his comments and suggestions. Finally, this paper was partially funded by the “Programa de Estímulo a la Excelencia Institucional (PEEI)”-University of Chile.

[2] http://energynumbers.info/capacity-factors-at-danish-offshore-wind-farms.

References

[1] R. De Vos, J. Sawin, Chapter One – Global and Regional Trends in Renewable Energy, in: Ready: Renewable Energy Action on Deployment, 2012, pp. 3–28.

[2] GWEC, Global Wind Report Annual Market Update 2014, 2015. Available: http://www.gwec.net/wp-content/uploads/2015/03/GWEC_Global_Wind_2014_Report_LR.pdf (accessed 24.09.15).

[3] A. Sahin, Progress and recent trends in wind energy, Prog. Energy Combust. Sci. 30 (2004) (2004) 501–543.

[4] EWEA, The Economics of Wind Energy, 2009. Available: http://www.ewea.org/fileadmin/files/library/publications/reports/Economics_of_Wind_Energy.pdf (accessed 24.09.15).

[5] M. Kapsali, J. Kaldellis, Offshore wind power Basics, cap. 2.14, pp. 431–468, in: A. Sayigh (Ed.), Comprehensive Renewable Energy, 2Elsevier, Oxford, Reino Unido, 2012, p. 36.

[6] S. Rodrigues, C. Restrepo, E. Kontos, R. Texeira, P. Bauer, Trends of offshore wind projects, Renew. Sustain. Energy Rev. 49 (2015) 1114–1135.

[7] A. Myhr, C. Mjerkseter, S. Ågornes, A. Nyaard, Levelised cost of energy for offshore floating wind turbines in a life cycle perspective, Renew. Energy 66 (2014) 71–728.

[8] EWEA, The European Wind Industry-key Trends and Statistics 2014, 2014. Available: http://www.ewea.org/fileadmin/files/library/publications/statistics/EWEA-European-Offshore-Statistics-2014.pdf (accessed 19.08.15).

[9] E. Zountouridou, G. Kiokes, S. Chakalis, P. Georgilakis, N. Hatziargyriou, Offshore floating wind parks in the deep waters of Mediterranean Sea, Renew. Sustain. Energy Rev. 51 (2015) 433–448.

[10] C. Hasager, A. Mouchem, M. Badger, F. Bingöl, I. Karagali, T. Driesenaar, A. Stoffelen, A. Peña, N. Longépé, Offshore wind climatology based on synergetic use of Envisat ASAR, ASCAT and QuikSCAT, Remote Sens. Environ. 156 (2015) 247–263.

[11] C. Hasager, A. Peña, M. Bruun, P. Astrup, M. Nielsen, F. Monaldo, D. Thompson, P. Nielsen, Remote sensing observation used in offshore wind energy, IEEE J. Sel. Top. Appl. Earth Obs. Remote Sens. (2008) 67–79.

[12] I. Karagali, A. Peña, M. Badger, C. Hasager, Wind characteristics in the North and Baltic Seas from the QuikSCAT satellite, Wind Energy 17 (2014) 123–140.

[13] R. Chang, R. Zhu, M. Badger, C. Hasager, R. Zhou, D. Ye, X. Zhang, Applicability of synthetic aperture radar wind retrievals on offshore wind resources assessment in Hangzhou Bay, China, Energies 7 (5) (2014) 3339–3354.

[14] E. Sharp, P. Dodds, M. Barret, C. Spataru, Evaluating the accuracy of CFSR reanalysis hourly wind speed forecasts for the UK, using in situ measurements and geographical information, Renew. Energy 77 (2015) 527–538.

[15] S. Rose, J. Apt, What can reanalysis data tell us about wind power? Renew. Energy 85 (2015) 963–969.

[16] M. Dvorak, B. Corcoran, J. Ten, N. McIntyre, M. Jacobson, US East coast offshore wind energy resources and their relationship to peak-time electricity demand, Wind Energy 16 (2013) (2013) 977–997.

[17] F. Pimenta, W. Kempton, R. Garivine, Combining meteorological stations and satellite data to evaluate the offshore wind power resource of Southeastern Brazil, Renew. Energy 33 (2008) 2375–2387.

[18] R. Chang, R. Zhum, M. Badger, C. Hasager, X. Xing, Y. Jiang, Offshore wind resources assessment from multiple satellite data and WRF modeling over South China sea, Remote Sens. (2015) 467–487.

[19] Y. Ping, Z. Shu, C. Nan, X. Zhirong, Offshore wind resouce assessment based on WRF model, in: Power and Energy Engineering Conference (APPEEC), 2013 IEEE PES Asia-Pacific (8–11 Dec. 2013, Kowloon, China), 2013.

[20] D. Carvalho, A. Rocha, M. Gómez, C. Santos, Sensitivity of the WRF model wind simulation and wind energy production estimates to planetary boundary layer parameterizations for onshore and offshore areas in the Iberian Peninsula, Appl. Energy 135 (2014) (2014) 234–246.

[21] D. Carvalho, A. Rocha, M. Gómez, C. Santos, WRF wind simulation and wind energy production estimates forced by different reanalyses: comparison with observed data for Portugal, Appl. Energy 117 (2014) (2014) 116–126.

[22] D. Carvalho, A. Rocha, M. Gómez-Gesteira, C. Silva, Offshore wind energy resource simulation forced by different reanalyses: comparison with observed data in the Iberian Peninsula, Appl. Energy 134 (2014) 57–64.

[23] A. Hahmann, C. Vincent, A. Peña, J. Lange, C. Hasager, Wind climate estimation using WRF model output: method and model sensitivities over the sea, Int. J. Climatol. 35 (12) (2014) 3422–3439.

[24] N. Nawri, G. Nína, H. Bjornsson, A. Hahmann, K. Jónasson, C. Hasager, N. Clausen, The wind energy potential of Iceland, Renew. Energy 69 (2014) (2014) 290–299.

[25] D. Watts, D. Jara, Statistical analysis of wind energy in Chile, Renew. Energy 36 (2011) (2011) 1603–1613.

[26] L. Morales, F. Lang, C. Mattar, Mesoscale wind speed simulation using CALMET model and reanalysis information: an application to wind potential, Renew. Energy 48 (2012) (2012) 57–71.

[27] DGF, Explorador Eólico Versión 2012, 2012. Available: http://ernc.dgf.uchile.cl/Explorador/Eolico2/info/Documentacion_Explorador_Eolico_V2_Full.pdf (accessed 23.06.15).

[28] C. Mattar, N. Villar, Estimación del potential eólico offshore en las costas de Chile utilizando datos de escaterómetro y Reanalysis, Rev. teledetec. 41 (2014) 49–58.

[29] R. Garreaud, R. Muñoz, The low-Level Jet off the West coast of subtropical South America: structure and variability, Mon. Weather Rev. 133 (2005) (2005) 2246–2261.

[30] CNE, Prospección eólica en zonas de las regiones de Atacama, de Coquimbo y del Maule, 2007. Available: http://www.cne.cl/archivos_bajar/Informe1_campana_III-IV.pdf (accessed 08.07.15).

[31] W. Skamarock, J. Klemp, J. Dudhia, D. Gill, D. Barker, M. Duda, et al., A Description of the Advanced Research WRF Version 3. *Technical Report* NCAR/TN–475+STR, NCAR 2008, 2008. Available: http://www2.mmm.ucar.edu/wrf/users/docs/arw_v3.pdf (accessed 24.09.15).

[32] J. Rutllant, R. Muñoz, R. Garreaud, Meteorological observations on the northern Chilean coast during VOCALS-Rex, Atmos. Chem. Phys. 13 (2013) (2013) 3409–3422.

[33] D. Dee, S. Uppala, A. Simmons, P. Berrisford, P. Poli, S. Kobayashi, et al., The ERA-Interim reanalysis: configuration and performance of the data assimilation system, Q. J. R. Meteorological Soc. 137 (2011) (2011) 553–597.

[34] D. Carvalho, A. Rocha, M. Gómez, Ocean surface wind simulation forced by different reanalyses: comparison with observed data along the Iberian Peninsula coast, Ocean Model. 56 (2012) (2012) 31–42.

[35] E. Giannakopoulou, R. Nhili, WRF model methodology for offshore wind energy applications, Adv. Meteorology 2014 (2014) (2014).

[36] D. Zafirakis, A. Paliatsos, J. Kaldellis, Energy yield of contemporary wind turbines, cap. 2.06, pp. 113–168, in: A. Sayigh (Ed.), Comprehensive Renewable Energy, 2Elsevier, Oxford, United Kingdom, 2012, p. 55.

[37] S. Shimada, T. Ohsawa, Accuracy and characteristics of offshore wind speeds simulated by WRF, SOLA 7 (2011) (2011) 021–024.

[38] H. Ross, J. Cooney, M. Hinzmann, S. Smock, G. Sellhorst, E. Dlugi, et al., Wind power potential in interior Alaska from a micrometeorological perspective, Atmos. Clim. Sci. 4 (2014) (2014) 100–121.

[39] D. Carvalho, A. Rocha, M. Gómez, C. Santos, A sensitivity study of the WRF model in wind simulation for an area of high wind energy, Environ. Model. Softw. 33 (2012) (2012) 23–34.

[40] D. Muñoz-Esparza, J. Van Beeck, B. Cañadillas, Impact of turbulence modeling on the performance of WRF model for offshore short-term wind energy applications, in: 13th International Conference on Wind Engineering. (13°, 10–15 July 2011, Amsterdam, Netherlands), 2011.

[41] A. Peña, A. Hahmann, C. Hasager, F. Bingöl, I. Karagali, J. Badger, et al., South Baltic Wind Atlas, 2011. Available: http://www.southbaltic-offshore.eu/reports-studies/img/SBO_Wind-Atlas.pdf (accessed 24.09.15).